Available online at www.sciencedirect.com
ScienceDirect
Ceramics International 36 (2010) 507–512
CERAMICS INTERNATIONAL
www.elsevier.com/locate/ceramint

TEM study of a fluorite-type $(1-x)Bi_2O_3{\cdot}xFe_2O_3$ superstructure in $BiFeO_3$ ceramics synthesized by the rapid liquid-phase sintering method

Chao Guo [a,b], Shizhou Pu [a,b], Zhenlian Chen [a], Meiya Li [a], Jiefeng Cao [a], Huamin Zou [a,b,*]

[a] Key Laboratory of Acoustic and Photonic Material and Device, Ministry of Education, Department of Physics, Wuhan University, Wuhan 430072, People's Republic of China
[b] Centre for Electron Microscopy, Wuhan University, Wuhan 430072, People's Republic of China

Received 4 June 2009; received in revised form 17 July 2009; accepted 4 September 2009
Available online 12 October 2009

Abstract

A commensurate modulated structure of $(1-x)Bi_2O_3{\cdot}xFe_2O_3$ is found in the $BiFeO_3$ ceramics synthesized by the rapid liquid-phase sintering method. Transmission electron microscopy studies show that the superstructure is based on fluorite-type δ-Bi_2O_3 and modulated probably by oxygen vacancy ordering. The existence of such a superstructure may increase the leakage current of $BiFeO_3$ ceramics.

Keywords: A. Sintering; B. Electron microscopy; Microstructure; Ferroelectric

1. Introduction

Multiferroic materials have been intensively investigated in recent years because they possess the properties of (anti)-ferroelectricity, (anti)ferromagnetism or even ferroelasticity simultaneously due to the coupling between ferroelectric and magnetic orders within one phase [1,2]. The $BiFeO_3$ system is one of the most studied multiferroic materials since it has a ferroelectric order below a Curie temperature of about 820 °C and an antiferromagnetic order below a Néel temperature of about 370 °C [3]. A large amount of doped or un-doped $BiFeO_3$ ceramics have been synthesized and reported. However, as pointed out by Scott, some of them have banana-type hysteresis loops which actually have nothing to do with the true ferroelectric properties [4]. Such artifacts may be due to the large leakage current induced by mixed valence of Fe ions, or by oxygen vacancies. It is known that point defects like ion vacancies, interstitials and substitutions in the bulk of material are responsible for many physical properties [5]. Thus, it is necessary to investigate the structures in $BiFeO_3$ ceramics more carefully before their properties are characterized.

A lot of doped and un-doped $BiFeO_3$ ceramics are prepared by the rapid liquid-phase sintering method (RLPS), because this method is said easier to produce single phase bulks [6–8]. However, the bulk may not be true single phase since some second phases may really exist but they are not detectable by X-ray diffraction (XRD). We synthesized four $BiFeO_3$ ceramics by RLPS, and measured the hysteresis loops. They all looked to be the unwanted banana-type (take the La and V doped $BiFeO_3$ ceramic for an example, see Fig. 1). Generally, $Bi_2Fe_4O_9$ and $Bi_{25}FeO_{39}$ are thought to present in the Fe-rich and Bi-rich regions, respectively, and affect the physics of the bulk by some extent [9]. However, our transmission electron microscopy (TEM) observations show that not only $Bi_2Fe_4O_9$ and $Bi_{25}FeO_{39}$, but also another phase exists in the bulks, which may greatly influence the polarization–electric field (*P–E*) measurements.

In the present paper, the results of TEM studies of $BiFeO_3$ ceramic bulks synthesized by RLPS are reported. It is found that a fluorite-type superstructure exists in all the samples. This second phase is based on δ-Bi_2O_3 which has a defect fluorite-type structure with only 75% oxygen sites statistically occupied. Selecting area electron diffraction (SAED), high resolution electron microscopy (HREM) and energy dispersion spectroscopy (EDS) were performed to determine this superstructure. Its influence on the electric property of $BiFeO_3$ ceramics is also discussed.

* Corresponding author at: Department of Physics, Wuhan University, Wuhan 430072, People's Republic of China.
E-mail address: hmzou@whu.edu.cn (H. Zou).

0272-8842/$36.00
doi:10.1016/j.ceramint.2009.09.023

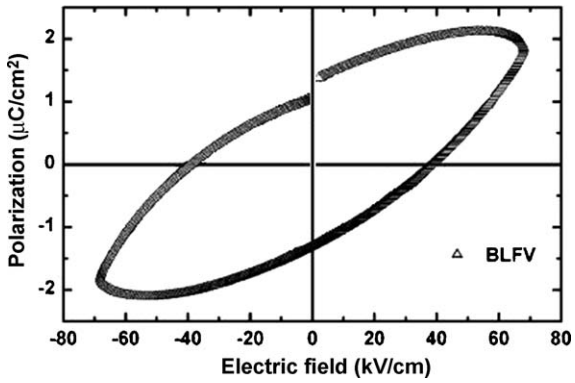

Fig. 1. The polarization–electric field loop of the BLFV ceramic at a frequency of 100 Hz.

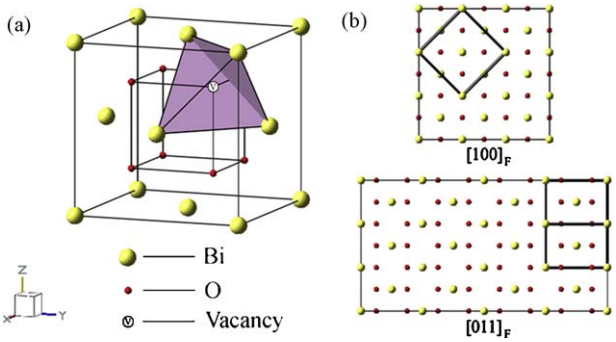

Fig. 2. (a) The structure of fluorite-type δ-Bi_2O_3 which has an oxygen vacancy. (b) The relationship between unit cells of the superstructure and fluorite-type δ-Bi_2O_3. The unit cell of basic fluorite is outlined with thick black lines.

2. Experimental

Four kinds of ceramic bulks were studied in our work: the un-doped $BiFeO_3$ (BFO), $Bi_{0.85}Ce_{0.15}FeO_3$ (BCF), $Bi_{0.85}La_{0.15}FeO_3$ (BLF) and $Bi_{0.85}La_{0.15}Fe_{0.97}V_{0.03}O_3$ (BLFV). All of them were prepared by the rapid liquid-phase sintering process as reported [10]. High purity starting powders of Bi_2O_3, Fe_2O_3, CeO_2, La_2O_3 and V_2O_5 were mixed in an agate mortar with distilled water according to the stoichiometric compositions, and then milled for 10 h at a rate of 250 rounds per minute. Afterwards, each powder mixture was pressed into discs with 1 mm in thickness and 15 mm in diameter at a pressure of 120 MPa with distilled water as the binder. The discs were dehydrated at 100 °C for 24 h, and then sintered in air at 880 °C for 7 min, and cooled down at a rate of about 40 °C/s. During the rapid firing process, Bi_2O_3 and possible few $Bi_{25}FeO_{39}$ (their melting points are 825 °C and 785 °C, respectively) melt before they react completely with Fe_2O_3 to form $BiFeO_3$. Hence, the method is called rapid liquid-phase sintering [9]. For TEM observations, the discs were mechanically ground down to 25 μm, and further argon ion milled to being transparent for the electron beam. The SAED was performed at the JEM-2010HT electron microscope for larger angle tilting of the sample, and the HREM observations were performed at the JEM-2010UHR electron microscope equipped with a field emission gun and the Ω-type energy filter. The operated accelerating voltages were both 200 kV. The EDS data was collected by the EDAX accessory on JEM-2010UHR. All observations were performed at room temperature.

3. Results and discussion

Fig. 2(a) shows the defect structure model of fluorite-type δ-Bi_2O_3. Bi atoms compose an fcc cubic sublattice, and O atoms occupy the centers of eight bismuth tetrahedrons. The eight tetrahedrons lose oxygen anions randomly, and thus produce oxygen vacancies as the one shown in Fig. 2(a). In the phase of δ-Bi_2O_3, only 75% oxygen sites are randomly occupied. It is known that δ-Bi_2O_3 is a high temperature form of bismuth oxide and cannot be quenched to room temperature [11–13]. However, by adding a certain amount of oxide MO_x (M = Nb, V, Mo, W, La, etc.), the fluorite-type phases based on δ-Bi_2O_3 can be obtained at room temperature [11–15]. In our bulks, a stable fluorite-type superstructure is produced during the synthesizing process.

The superstructure was found in many crystallites when we were studying the $BiFeO_3$ ceramics using SAED. The electron diffraction patterns (EDPs) of the superstructure in our BCF ceramic are shown in Fig. 3(a)–(d). They are observed along $[1\,0\,0]_F$, $[0\,1\,0]_F$, $[2\,3\,3]_F$, $[0\,1\,1]_F$ zone axis orientations, respectively. Here, the subscript 'F' means that the zone axes are indexed according to the fluorite structure. In each pattern, the strongest diffraction spots originate from the average structure, and are indexed based on the fluorite subcell. Besides the main spots, there are many weak spots in EDPs. These satellite spots contain information about the superstructure. It is seen that the modulation is commensurate. Thus, by all EDPs, we define a unit cell of the superstructure whose volume is $(3/2)\sqrt{2} \times (3/2)\sqrt{2} \times 4$ times as large as that of the basic fluorite unit cell as shown in Fig. 2(b). The fluorite unit cell is outlined with thick black lines. Fig. 3(e) and (f) are the $[0\,1\,1]_F$ EDPs of superstructure found in BFO and BLFV ceramics, respectively. They have almost the same periodicity as that in BCF. In BLF and other previously mentioned ceramics synthesized in different batches, we also observed similar EDPs of the superstructure. Therefore, it seems that the existence of superstructure has no relation with the dopants, but has relation with the sintering method and the two main materials: Bi_2O_3 and Fe_2O_3.

To fully understand the superstructure, HREM experiments were performed. Fig. 4 shows a HREM image of BCF ceramic along $[0\,1\,1]_F$. The result of EDS given below will show that there exist almost no Ce in the superstructure grains as can be seen from Fig. 8(a). In the thin region A near a hole, almost no stripe is observed. While, in the thicker region B, some stripes with slight contrast come to be visible. In the Fourier transform of whole pattern, a few satellite spots can be seen, besides the basic strong spots. The simulated HREM image of fluorite-type δ-Bi_2O_3 along $[0\,1\,1]_F$ (thickness $t = 20$ Å and defocus $\Delta f = -225$ Å) agrees very well with the enlarged HREM image from region A, which confirms that the basic structure of the crystal is fluorite-type δ-Bi_2O_3. The reason that no modulation strips appear in region A lies on that, the modulation is most likely to be induced by oxygen vacancy

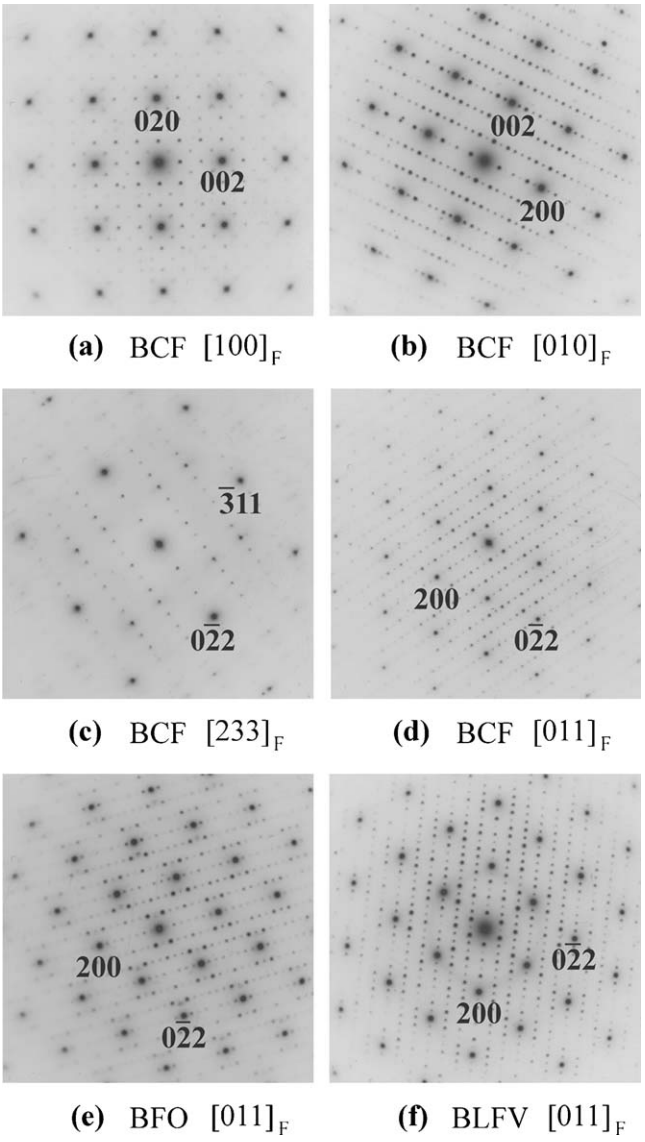

Fig. 3. (a)–(d) The EDPs of superstructure in BCF ceramics along $[1\,0\,0]_F$, $[0\,1\,0]_F$, $[2\,3\,3]_F$, $[0\,1\,1]_F$ zone axis, respectively. (e) and (f) The EDPs of superstructure along $[0\,1\,1]_F$ zone axis in BFO and BLFV ceramics, respectively.

ordering, and the weak potential change due to the different occupation probability of oxygen atoms is enhanced by the dynamical scattering effect in relatively thick region [16].

Fig. 5 shows the HREM image along $[0\,1\,1]_F$ taken from a much thicker region of the same grain as Fig. 4. To reduce the noise induced by amorphous layers, the Wiener filter is applied to this image. The modulation stripes are visible in the whole image. In the Fourier transform shown in Fig. 5, dense satellite spots are clearly seen, which is the same as the $[0\,1\,1]_F$ EDP. Unfortunately, this HREM image cannot be directly used to illustrate the ordered arrangement of atoms by the contrast, because the thickness is too large and the weak-phase-object approximation is not valid in this case. However, by investigating the periodicity of dot brightness, more information of the superstructure can still be figured out. It is seen in region C that the contrast of stripes is stair-like arranged. By

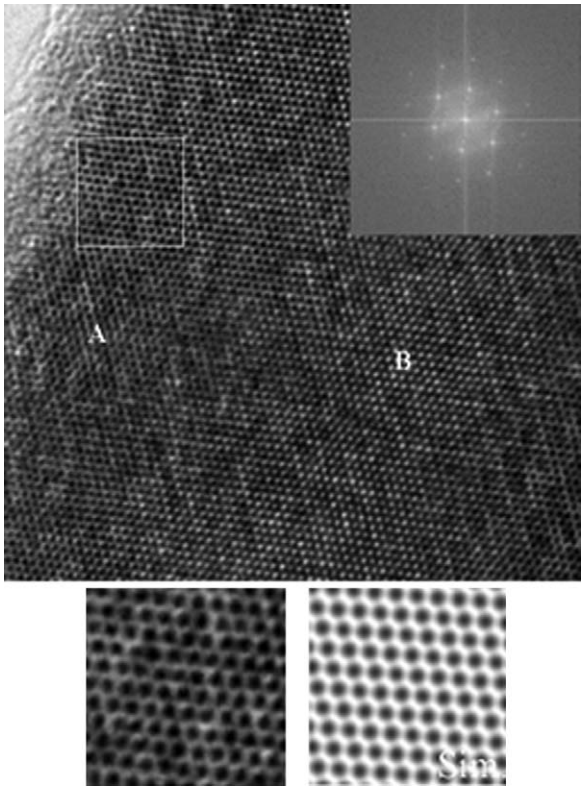

Fig. 4. The HREM image of a superstructure crystallite along $[0\,1\,1]_F$ in the BCF ceramic. The inset image at top right corner is the Fourier transform of whole pattern. A part of image within the white square in region A is enlarged, and a simulation of fluorite-type δ-Bi_2O_3 with thickness $t = 20$ Å and defocus $\Delta f = -225$ Å is displayed for comparison.

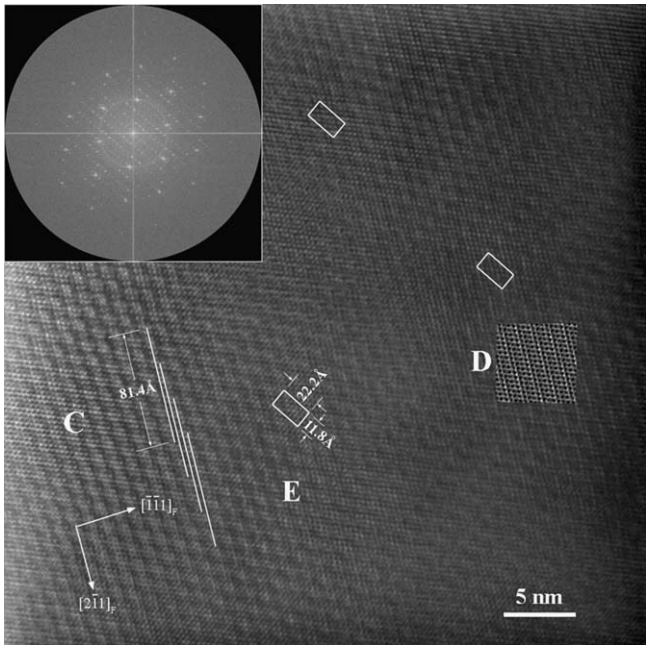

Fig. 5. The HREM image of the same superstructure crystallite along $[0\,1\,1]_F$ in a thicker area. The inset image at top left corner is the Fourier transform of whole pattern. The white rectangles represent the unit cells of superstructure. The long white lines illustrate the stair-like arrangement of the periods in $(1\,1\,\bar{1})_F$ plane of dot contrast. A copy of simulated HREM image with $\Delta f = -200$ Å and $t = 70.5$ Å in Fig. 7 is displayed in region D for comparison.

careful investigation, it is found that the period of dot contrast along $[2\,\bar{1}\,1]_F$ direction covers 24 dots as shown by the white lines. Each dot represents one column of Bi(Fe) atoms when only the spacing of repeated columns is considered. The same periodical distribution of the dot brightness is repeated in the next $(1\,1\,\bar{1})_F$ plane, but shifted toward $[2\,\bar{1}\,1]_F$ direction by 7 columns, over and over. The unit cell of the superstructure defined by above EDPs is marked with the white rectangle outline in three different areas. It also covers 24 dots, and thus agrees with the stair-like stacking. But, the problem is how the variation of the dot brightness with period of 24 columns in $(1\,1\,\bar{1})_F$ plane is induced? The supposal that the oxygen vacancy ordering plays the main role in this phenomenon is based on the following reason. Cations in the perfect fluorite-type oxide are required to be tetravalent, while Bi and Fe cations are most likely to be trivalent. Hence, the oxygen deficiencies are needed. In region E, the feature of contrast variation within $(1\,1\,\bar{1})_F$ plane reveals that 12 brighter dots are succeeded by 12 darker (or blur) dots. Therefore, the oxygen vacancies are suggested to be arranged in the successive 12 columns of every 24 oxygen columns in $(1\,1\,\bar{1})_F$ plane. According to this idea and all EDPs, a model of the superstructure is proposed as shown in Fig. 6(a). The centers of dark triangles represent the oxygen columns which are partly occupied by vacancies. Fig. 6(b) illustrates the stair-like ordering of oxygen vacancies as above mentioned. The three black lines represent the white lines shown in Fig. 5. The sites of cations are supposed to be statistically occupied by 80% Bi and 20% Fe (Ce is neglected). Here, the ratio of Bi/Fe for calculation is approximately evaluated by EDS results below. According to this model, a series of simulated images with defocus values from −500 to −200 Å and thicknesses from 23.5 to 94 Å are displayed in Fig. 7. The image for $\Delta f = -200$ Å and $t = 70.5$ Å appears to agree well with the image in region D where the brighter stripes are clearly seen in the experimental image. Thus, the simulation confirms the possibility of oxygen vacancies ordering. It is seen that the appearances of the image in Fig. 5 are not consistent all over, though they have the same superstructure, which might indicate that the concentration of oxygen vacancies are different from a region to another region. This may be caused by the crystallization and composition fluctuation due to fast cooling down from the liquid phase in the process of RLPS.

The EDS technique is performed to study the chemical composition of the superstructure. Fig. 8(a) shows the spectrum of a crystallite that possesses the superstructure in BCF ceramic. For comparison, the spectrum of a normal $BiFeO_3$ grain in BFO ceramic is given in Fig. 8(b). Both the two spectrums are normalized to the Bi-Mα peak at 2.5 keV. It is seen that a great difference exists between the two spectra in the Fe-Kα peak at 6.4 keV. In Fig. 8(b), the intensity of Fe-Kα peak agrees with the Bi/Fe ratio of $BiFeO_3$. While, in the superstructure, the Fe-Kα peak is apparently much lower, which means that much smaller amount of Fe is mixed into the δ-Bi_2O_3 matrix. Also, there are even smaller peaks of dopant Ce visible in the spectrum, which indicates a neglectable amount of Ce doped in the superstructure crystallite. Moreover, since the superstructure is found in all of our ceramics including BFO, BCF, BLF and BLFV, the modulation is considered to be not related with dopants, but related with the direct thermal treatment (RLPS) of Bi_2O_3 and Fe_2O_3 mixture in some Bi-rich regions. That is, the chemical composition of superstructure

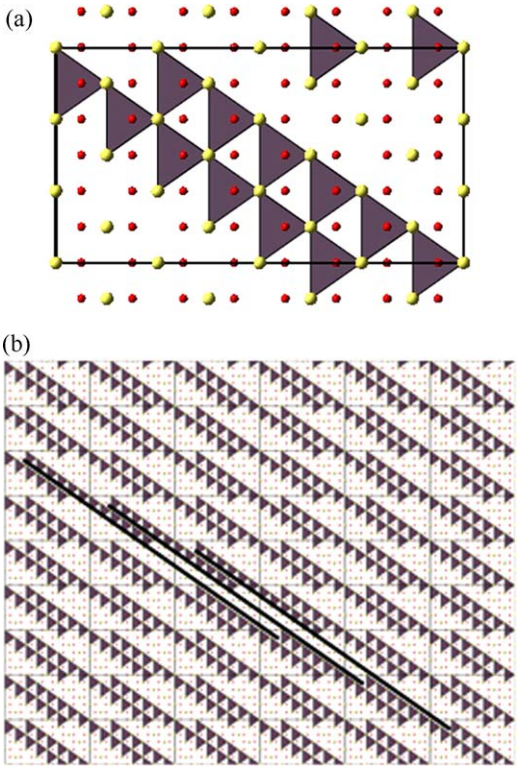

Fig. 6. (a) The supposed model of the unit cell of superstructure. The centers of dark triangles represent the oxygen columns which are partly occupied by vacancies. (b) Illustration of the stair-like ordering of oxygen vacancies. The thick black lines indicate the period of columns in $(1\,1\,\bar{1})_F$ plane.

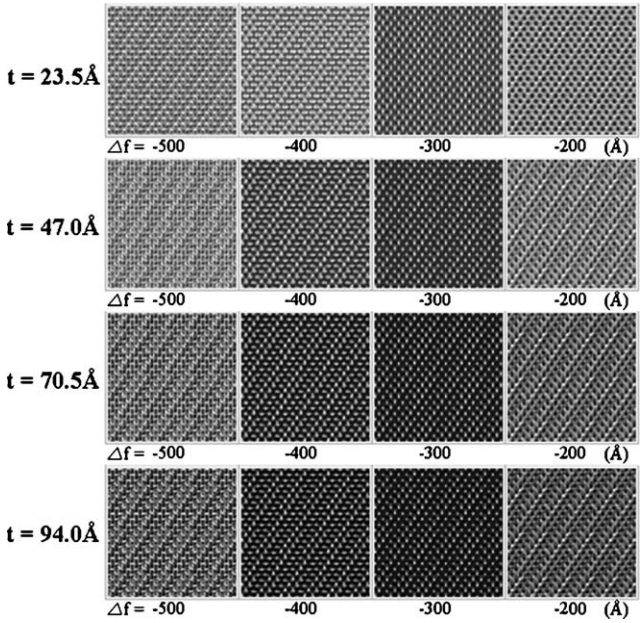

Fig. 7. The simulated images of superstructure along $[0\,1\,1]_F$ as functions of the thickness and defocus values.

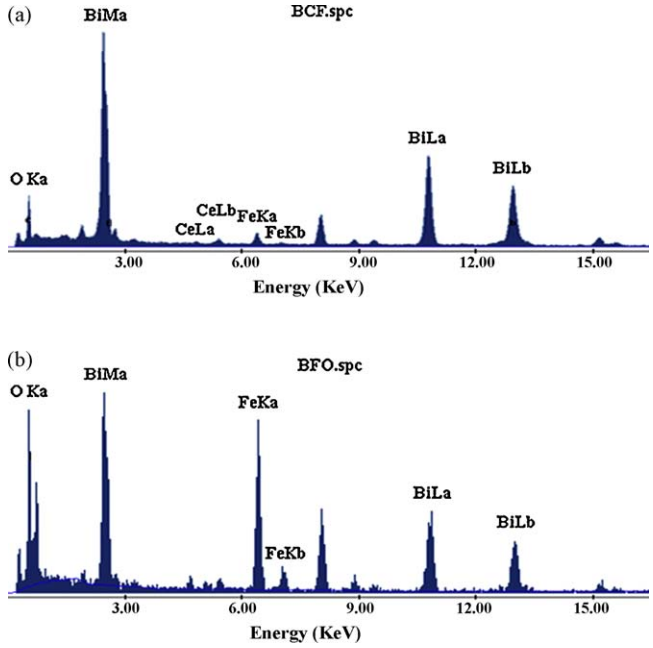

Fig. 8. (a) The EDS pattern of a superstructure crystallite in the BCF ceramic. (b) The EDS pattern of an un-doped $BiFeO_3$ crystallite for comparison.

should be $(1-x)Bi_2O_3{\cdot}xFe_2O_3$. The value of x is calculated according to the ratio of Bi/Fe from eight EDS spectra of four superstructure crystallites to be that, $0.19 \leq x \leq 0.22$. Finally, the O-Kα peaks between two spectrums are compared. It is clearly seen that the O-Kα peak at 0.52 keV in superstructure of Fig. 8(a) looks less than half of that in $BiFeO_3$ of Fig. 8(b). Suppose the O/Bi ratio in $BiFeO_3$ is around the ideal value of 3/1, the O/Bi ratio in superstructure should be much less than 2/1 (the ratio of O/Bi in defect-free fluorite structure), which confirms the existence of high concentration of oxygen vacancies.

According to the sample preparation and the observations on a series of ceramics, it is considered that the RLPS method is the key factor which affects the formation of the superstructure. The time for thermal treatment is limited to as little as several minutes, though the attempt is to reduce the formation of $Bi_2Fe_4O_9$ and $Bi_{25}FeO_{39}$. Thus, a part of Bi_2O_3 reacts with Fe_2O_3, and forms the superstructure before more Fe_2O_3 joins in to produce $BiFeO_3$ due to the fast cooling process. Since the superstructure is based on the fluorite-like δ-Bi_2O_3, the superstructure is easily mistaken for residual Bi_2O_3 in X-ray analysis when its concentration is small compared with $BiFeO_3$. While, we actually never find the structure of pure Bi_2O_3 in the ceramics synthesized by RLPS, but always find the superstructure.

The exact influences of the superstructure on the multiferroic properties of $BiFeO_3$ ceramics are still under inspection. However, it is noticed that, the hysteresis loops of the four ceramics are banana-type which is interpreted by Scott [4] as typical loss of dielectrics, and the leakage current density of BLFV is about two orders of magnitude lower than that of BLF specimen as measured by Yu et al. [10]. Since the oxygen deficient Bi_2O_3 is a well known ion conductor [17,18], it is reasonable to associate the large leakage current with the oxygen deficient Bi_2O_3. That is, the oxygen vacancies in the superstructure might increase the leakage current. Moreover, in the study of Qi et al., it is found that higher valency state of the dopant Ti^{4+} can greatly increase the dc resistivity compared with Ni^{2+} dopant in $BiFeO_3$ [19]. Kothari et al. also suggested that the doping of low-valent Ca^{2+} into $BiFeO_3$ causes the production of oxygen vacancies instead of Fe^{3+} changing to Fe^{4+} [20]. All these agree with the measuring results of the ceramics we used that the dopant V^{5+} can greatly reduce the leakage current compared with La^{3+} dopant in $BiFeO_3$ as reported [10]. Thus, it is reasonable to consider that the high-valent dopants introduce more oxygen and partially fill the vacancies, which reduces the vacancy concentration. Therefore, it is necessary to improve the synthesizing method for $BiFeO_3$ ceramics to prevent from the formation of the new phase of $(1-x)Bi_2O_3{\cdot}xFe_2O_3$ superstructure.

4. Conclusions

In this paper, we report a fluorite-type superstructure in the multiferroic $BiFeO_3$ system ceramics synthesized by the RLPS method. This second phase is easy to be misinterpreted as residual Bi_2O_3. But our EDP and HREM studies show that this phase possesses a commensurate modulated structure which is probably induced by oxygen vacancy ordering. The EDS results indicate that the superstructure is mainly composed of Bi_2O_3 and Fe_2O_3. This second phase which is rich in oxygen vacancies will cause the large leakage current, and makes the measured ferroelectric hysteresis loop be a banana-type.

Acknowledgement

The authors wish to express their sincere thanks to Dr. Benfang Yu (Department of Physics, Wuhan University, China) for rendering the $BiFeO_3$ ceramics investigated in this paper.

References

[1] W. Eerenstein, N.D. Mathur, J.F. Scott, Nature 442 (2006) 759.
[2] W. Prellier, M.P. Singh, P. Murugavel, J. Phys.: Condens. Matter 17 (2005) 803.
[3] G.A. Smolenskii, I.E. Chupis, Sov. Phys. Usp. 25 (1982) 475.
[4] J.F. Scott, J. Phys.: Condens. Matter 20 (2008) 021001.
[5] S. Ling, Phys. Rev. B 49 (1994) 864.
[6] Y.P. Wang, L. Zhou, M.F. Zhang, X.Y. Chen, J.M. Liu, Z.G. Liu, Appl. Phys. Lett. 84 (2004) 1731.
[7] G.L. Yuan, S.W. Or, Y.P. Wang, Z.G. Liu, J.M. Liu, Solid State Commun. 138 (2006) 76.
[8] A.K. Pradhan, K. Zhang, D. Hunter, J.B. Dadson, G.B. Loutts, P. Bhattacharya, R. Katiyar, J. Zhang, D.J. Sellmyer, U.N. Roy, Y. Cui, A. Burger, J. Appl. Phys. 97 (2005) 93903.
[9] M. Valant, A.K. Axelsson, N. Alford, Chem. Mater. 19 (2007) 5431.
[10] B.F. Yu, M.Y. Li, J. Liu, D.Y. Guo, L. Pei, X.Z. Zhao, J. Phys. D: Appl. Phys. 41 (2008) 065003.
[11] C.D. Ling, R.L. Withers, S. Schmid, J.G. Thompson, J. Solid State Chem. 137 (1998) 42.
[12] C.D. Ling, M. Johnson, J. Solid State Chem. 177 (2004) 1838.
[13] D. Tang, W. Zhou, J. Solid State Chem. 119 (1995) 311.

[14] A. Castro, E. Aguado, J.M. Rojo, P. Herrero, R. Enjalbert, J. Galy, Mater. Res. Bull. 33 (1998) 31.
[15] M. Wołcyrz, L. Kępiński, R. Horyń, J. Solid State Chem. 116 (1995) 72.
[16] K. Hiraga, T. Oku, D. Shindo, M. Hirabayashi, J. Electron Microsc. Tech. 12 (1989) 228.
[17] T. Takahashi, H. Iwahara, Mater. Res. Bull. 13 (1978) 1447.
[18] A.W. Sleight, Science 208 (1980) 895.
[19] X.D. Qi, J. Dho, R. Tomov, Appl. Phys. Lett. 86 (2005) 062903.
[20] D. Kothari, V.R. Reddy, A. Gupta, V. Sathe, A. Banerjee, S.M. Gupta, A.M. Awasthi, Appl. Phys. Lett. 91 (2007) 202505.